Progress in Additive Manufacturing (2019) 4:197–209
https://doi.org/10.1007/s40964-019-00088-4

FULL RESEARCH ARTICLE

Direct coupling of fixed screw extruders using flexible heated hoses for FDM printing of extremely soft thermoplastic elastomers

Mohammad Abu Hasan Khondoker[1] · **Dan Sameoto**[1]

Received: 25 June 2018 / Accepted: 20 June 2019 / Published online: 29 June 2019

Abstract
We present a new method—fused pellets printing—to print any thermoplastic materials by converting a screw extruder into a direct source for feeding material into fused deposition modeling (FDM) style 3D printer. We achieve this by feeding thermoplastic pellets into a stand-alone single screw system that melts and pushes the material through a flexible heated hose to the print head. The material is finally deposited through the print head onto the print bed to construct the 3D object. This heated hose decouples the large mass extruder from an FDM print head which can then move with high speed and precision. The result is a very simple 3D printing tool that can take raw input pellets or even recycled thermoplastic scrap, and directly print parts without the need to produce an intermediate, high-quality filament. This technique has been successfully used for pellets of both soft and hard thermoplastics. Using pellets of styrene–ethylene–butylene–styrene, airtight pneumatic soft robotic actuators have been printed in a single process. In theory, this technique should be suitable for any thermoplastic material regardless of their flexibility, stretchability, and hardness which is not possible with currently available commercial FDM systems.

Keywords Fused deposition modeling · Additive manufacturing · Fused pellet printing · Thermoplastic elastomer · Pellet extruder

1 Introduction

Fused deposition modeling (FDM) is an additive manufacturing (AM) technique where a molten material is extruded through a nozzle to develop two-dimensional (2D) layers. Each layer is deposited onto the previously deposited layer, thus constructing the whole three-dimensional (3D) object [1]. In general, in FDM, the feed material is provided as a previously formed filament from a roll, with full control over the feed rate by virtue of a motor-roller feeder assembly. Then, the filament is liquefied inside a melt chamber and then extruded through a nozzle. The melt chamber and the nozzle assembly are commonly known as the hot end.

Electronic supplementary material The online version of this article (https://doi.org/10.1007/s40964-019-00088-4) contains supplementary material, which is available to authorized users.

✉ Mohammad Abu Hasan Khondoker
khondoke@ualberta.ca

[1] Department of Mechanical Engineering, University of Alberta, 10-390, Donadeo Innovation Centre for Engineering, Edmonton T6G 1H9, Canada

The filament between the spool and roller assembly is in tension, whereas, between the roller and melt chamber, the filament is in compression [2]. Three major factors control the operation of a motor-roller feeder assembly—the maximum torque supplied by the feeder motor, the amount of force transferred from the motor shaft to the solid filament, and the column strength of the filament before entering the melt chamber [3].

The main driving force is the torque (τ) supplied by the feeder stepper motor. Here, the solid filament acts as a piston to push the highly viscous polymer melt through the print nozzle. The required motor power (P_{motor}) can be estimated from Eq. 1 [4–6]:

$$P_{\text{motor}} = \frac{1}{2}\Delta P A \omega_{\text{r}} R_{\text{r}}, \tag{1}$$

where ΔP is the pressure drop in the melt chamber, A is the cross-sectional area of the filament, and ω_{r} and R_{r} are the angular speed and radius of the toothed gear of the driving motor. The coefficient of friction (f) between counter-rotating wheels and the filament determines how much force can be transferred to the filament from the motor shaft. Elkins

et al. showed that, due to the larger coefficient of friction, use of a soft rubbery wheel resulted in higher force transferred to the filament when compared to a hard epoxy wheel [3]. While serving as a piston under compression, the filament must also have enough column strength (also known as axial rigidity) to avoid buckling between the motor-roller assembly and the melt chamber. A higher viscosity of the polymer melt increases the force on the solid filament that is required to push the molten polymer through the nozzle. This force cannot be supplied by the solid filament if the column strength is insufficient. The column strength can be estimated from the critical buckling pressure ($P_{\text{critical load}}$) using Euler's buckling theory as follows [7, 8]:

$$P_{\text{critical load}} = \frac{\pi^2 E d^2}{16 L^2}, \tag{2}$$

where, E, d, and L are the elastic modulus, diameter, and length of the solid filament between the rollers and the melt chamber. Hence, the solid filament must have high E or small L to overcome resistance within the hot end while not buckling or otherwise failing to feed. All of these requirements by the motor-roller feeder assembly limit how soft an input filament can be, and the majority of FDM printers are optimized for rigid filament materials like acrylonitrile butadiene styrene (ABS), polylactic acid (PLA), and high impact polystyrene (HIPS).

Specific applications such as soft robotics require 3D printing of soft elastomeric materials, which is challenging, because the column strength of their filament is often lower than the limit imposed by the rollers. Researchers have printed thermoplastic elastomers with a hardness of approximately 70 Shore A using a modified version of the feeder-roller assembly [3]. Commercially available semi-flexible FDM filaments, such as NINJAFLEX® [9], PolyFlex™ [10], and FlexSolid® [11], can be used in feeder-roller assembly, but are relatively stiff and may not be appropriate for certain low pressure or high deformation applications. If softer materials are to be used in FDM processing, alternatives to the filament feed system are required. There are at least one patented technique, some commercial solutions, and published reports where a mini-extruder mounted on the print head was exploited to 3D print directly from pellets [12–19]. However, having a pellet extruder directly attached to a print head increases its size and weight, requiring stronger components, and limiting the use of this feeding system in multi-material FDM printing. The direct mount pellet extruder also has issues with clogging the print material in the screw [15] and difficulty in immediate ON/OFF control of the melt flow [16]. Hence, it is of great interest to design a custom feeder system for FDM printers which can function for any thermoplastic materials, regardless of their hardness, and minimizes the extra loads placed on the linear stages and motors. Using such a feeder system, a multi-material FDM system would be able to directly print soft robots with different components made of materials with varying hardness, all in a single step.

Using a custom flexible heated hose, we demonstrate the newest 3D printing technology, fused pellets printing (FPP), a novel feeder system to print almost any thermoplastic material if it melts at a temperature below the maximum temperature rating of the thermistor/heater used in the system, i.e., 400 °C in this case. The following sections focus on the design and development of the heated hose feeder system and fine-tune the process parameters to achieve quality prints.

2 Experimental setups

An inexpensive FDM style 3D printer (Model: M201) was purchased from Geeetech, China. The original print head of this printer was a 2-in-1-out type hot end, which inputs two filaments to co-extrude them in a side-by-side manner or change the composition of the print in each new layer to be deposited. The original printer head was replaced by a custom tri-extruder system described in the following section. The pre-installed firmware of this printer also allows users to change the composition of the print at any time by regulating the relative feed rate of both polymers.

2.1 Materials

Soft thermoplastic elastomer pellets of Kraton G1657 (styrene ethylene butylene styrene (SEBS)) purchased from Kraton Corporation, USA were used as received. SEBS is a triblock copolymer composed of styrene end blocks and ethylene/butylene interior blocks. Kraton G1657 is optically transparent, which has a hardness of approximately 47 Shore A, and in its bulk form, it can stretch up to approximately 600% [20, 21]. In addition to elastomeric pellets, rigid pellets of MM3520 shape memory polymer (SMP) purchased from SMP Technologies Inc., Japan, were also successfully used in our system. This SMP has a hardness of 77 Shore D in its glassy state; however, by heating well above its glass transition temperature (35 °C), its hardness can be lowered to approximately 80 Shore A in its rubbery state.

2.2 Design of the print head

Direct printing from pellets comprises three major components: a pellet extruder, a flexible heated hose, and print head. The schematic diagram in Fig. 1a shows all the major components of FPP technology. The actual system is

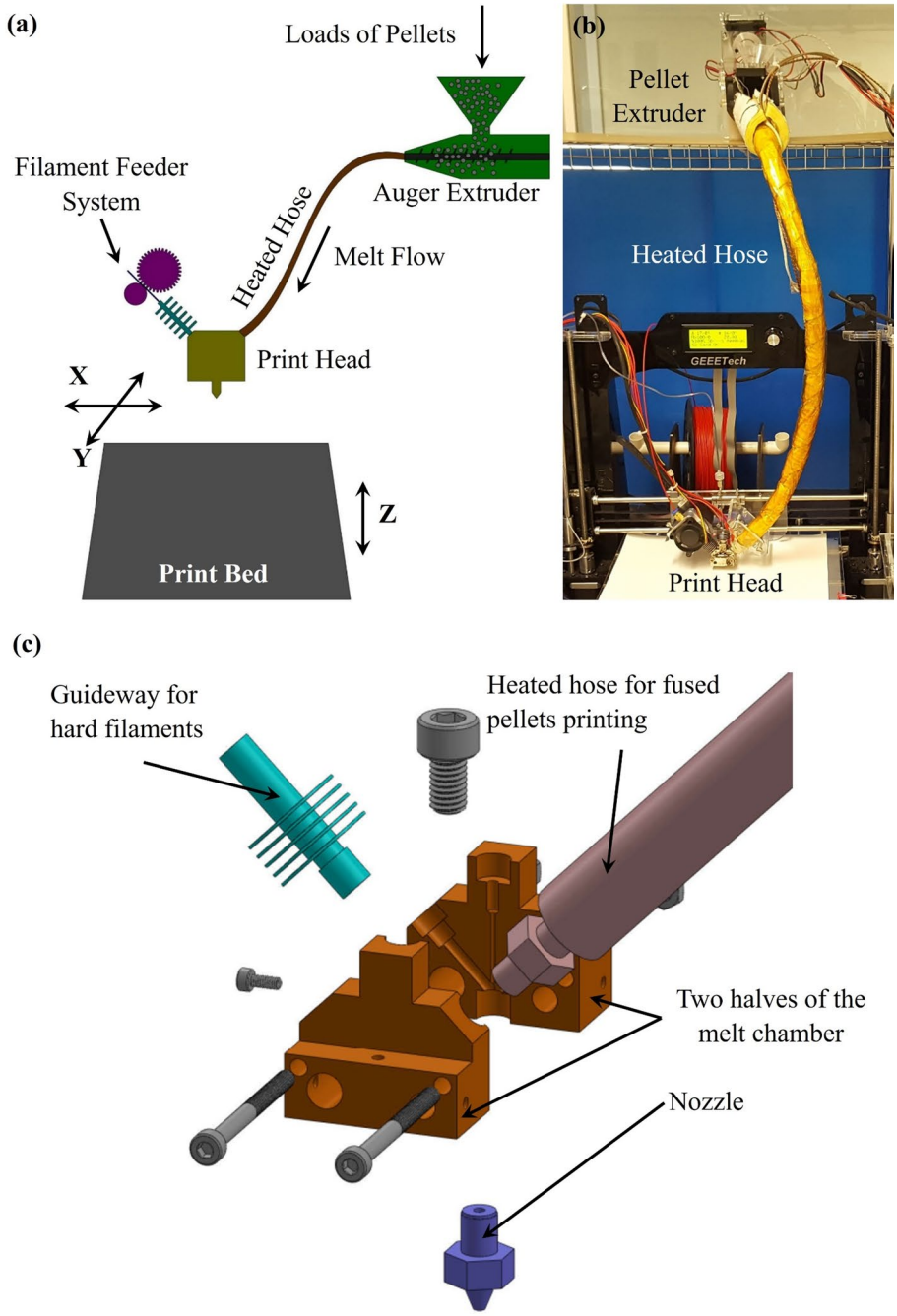

Fig. 1 **a** The schematic diagram of the fused pellets printing technology showing all three major components (i.e.) pellet extruder, flexible heated hose, and the print head, **b** the actual fused pellet printing system, and **c** the exploded 3D model of the tri-extruder print head

presented in Fig. 1b, and the exploded 3D model of the print head is shown in Fig. 1c.

2.2.1 Pellet extruder

The original pellet extruder [22] was bought from Filastruder, USA as a Do-It-Yourself (DIY) kit. This extruder uses a single screw (15.5 mm in diameter and 18 cm in length) with hex shank coupled with a GF45 series 12 VDC gearmotor (max 8 rpm and 15.6 Nm torque). The voltage and current supplied to the gearmotor can be regulated using a closed loop PWM controller to control the speed and torque of the gear motor, respectively. It enables the user to adjust the extrusion speed which mainly depends on extrusion temperature. The extrusion temperature was controlled using a collar heater on the barrel, a K-type surface mount thermocouple, and a PID controller.

2.2.2 Flexible heated hose

The 2-foot (0.61 m)-long flexible, heated hose is the major component which connects the pellet extruder with the

print head. A B-series 2-foot-long PTFE hose with 1/8 in (3.18 mm) nominal internal diameter (part number: SS-BT 2 TA2 TA2-24) was purchased from Swagelok, Canada. This hose has a PTFE core with 304 stainless steel braided cover. The hose has a maximum limit of working pressure of 206 bar (2.06×10^7 Nm^{-2}) rated at 20 °C and a maximum temperature of 230 °C, according to the manufacturer's specification. This maximum temperature puts a limit on input material choice for this system, but is sufficient for demonstrating the concepts. The hose has a 1/8 in (3.18 mm) Swagelok tube adapter on both ends, whereas both the pellet extruder and print head have M6 × 1 mm female thread opening. To fulfill the assembly requirement, ¼ in NPT (6.35 mm) male tube fittings were purchased and swaged to M6 × 1 mm male fitting. To ensure that the polymer melt remains in the molten state while being transported from the pellet extruder to the printing head, the hose must be kept above the melting temperature of the polymer at all time. For this purpose, the hose was first wrapped with a 4-foot (1.22 m) long, 120 VAC, 78 W flexible heat cable (part number: 4550T162) purchased from McMaster-Carr. Then, a K-type surface mount Ni probe thermocouple (part number: 9251T93) from McMaster-Carr was attached, so that it never touches the heat cable directly—rather, it maintains contact with the braided metal surface of the hose. Finally, a 3 mm-thick fiberglass insulation was wrapped around the tube and secured with an extra layer of Kapton tape. Using a separate PID controller, the temperature of this flexible, hot tube was controlled independently.

2.2.3 Print head

A custom tri-extruder, reported elsewhere [23, 24], was employed here which has three inputs. One input channel was attached with a regular motor-roller feeder assembly to feed filaments of rigid polymers. Another input channel was connected to the flexible heated hose to feed soft thermoplastic pellets using the FPP technology. The third input of this tri-extruder was kept inactive and is intended for future use.

2.3 Flow analysis

This system involves two major melt flows: single screw extrusion flow inside the barrel and laminar pipe flow through the heated hose. The physics of the single screw extrusion is well developed in the literature which consists of three types of flows [25], as shown in Fig. 2a. They are a drag flow, caused from the interaction of the rotating screw and stationary barrel, an opposing pressure flow due to the pressure gradient developed along the screw length, and a leakage flow through the clearance between screw and barrel, which reduces the overall output of the extruder. This leakage flow may be negligible

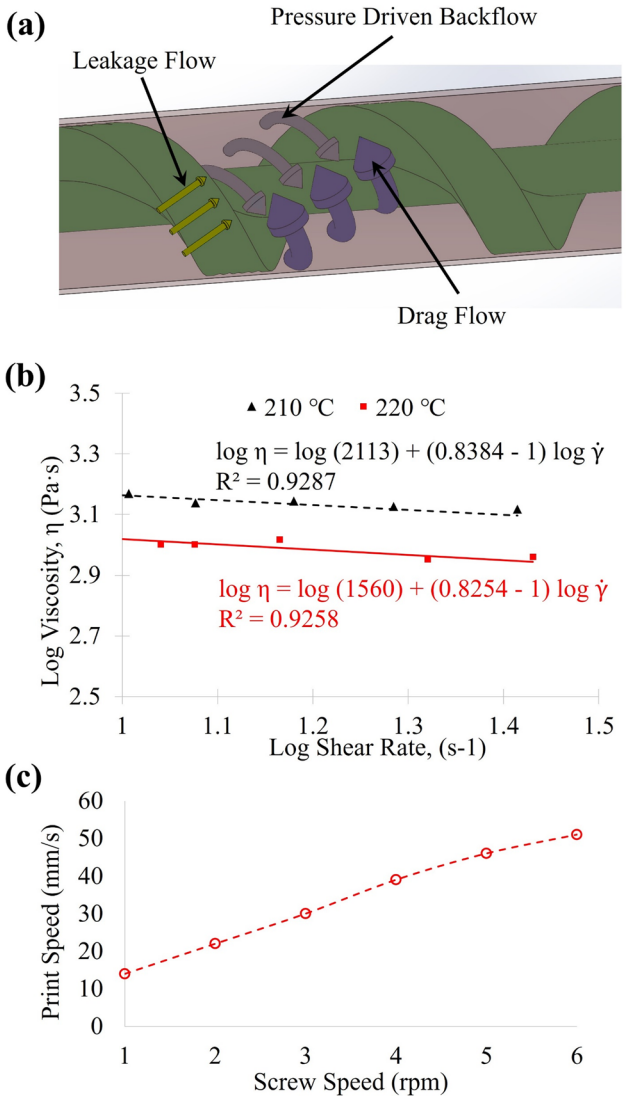

Fig. 2 **a** Illustration of three melt flows inside the screw system, **b** the flow curves of SEBS at 210 °C and 220 °C temperatures in a log–log scale, and **c** the variation in actual print speed using 0.5 mm nozzle at different screw speeds

if the screw is not significantly worn [26]. Apart from these flow components inside the extruder, there is another opposing pressure flow resulting from the pressure gradient developed within the heated hose. From the literature [27], the drag flow, Q_d, can be estimated using the following equation:

$$Q_d = \frac{1}{2} \times (\pi D \tan\phi - e) \times \left(\pi D \frac{N}{60} \cos^2\phi\right) \times H, \quad (1)$$

where the diameter of the screw $D = 15.5$ mm, helix angle $\phi = 35°$, flight width $e = 11$ mm, channel depth of the auger $H = 5.25$ mm, and $N =$ screw speed in rpm. Hence, for our system, drag flow (Q_d) reduces to the following:

$$Q_d = (3.3 \times 10^{-8} N)\ m^3/s. \quad (2)$$

The mathematical model for pressure flow inside the extruder has also been developed in the literature as follows [25, 27]:

$$Q_{\mathrm{p}} = \frac{wH^3 \sin\phi}{12\eta} \times \left(\frac{\mathrm{d}p}{\mathrm{d}L}\right)_{\mathrm{Extruder}}, \tag{3}$$

where the channel width of the screw, $w = (\pi D \tan\phi - e)\cos\phi = 18.92$ mm, η = viscosity of the polymer melt, and $\left(\frac{\mathrm{d}p}{\mathrm{d}L}\right)_{\mathrm{Extruder}}$ = the pressure gradient along the screw length inside the pellet extruder. This equation was derived for a Newtonian fluid which follows the simple linear viscosity relation, i.e., $\tau = \eta\dot{\gamma}$. However, polymer melts are highly non-linear viscoelastic fluids. Thus, it is reasonable to consider the power-law fit equation for the melt viscosity, assuming that the temperature is uniform throughout the extruder. Hence, we get the viscosity relation as follows [4]:

$$\eta = K\dot{\gamma}^{n-1}. \tag{4}$$

Here, K = consistency index and n = power-law index. These power-law fit parameters can be estimated from the viscosity curve (viscosity vs. shear) of the polymer melt. Therefore, using Eq. (4) in conjunction with the model developed by Crawford [26], the pressure flow equation has been re-formulated as follows. The detailed derivation can be found in the supplementary information:

$$\left(Q_{\mathrm{p}}\right)_{\mathrm{Extruder}} = \frac{2nw}{(2n+1)} \times \sqrt[n]{\frac{\sin\phi}{K}\left(\frac{\mathrm{d}p}{\mathrm{d}L}\right)_{\mathrm{Extruder}}} \times \left(\frac{H}{2}\right)^{\left(\frac{2n+1}{n}\right)}. \tag{5}$$

Using an HAAKE™ Minilab twin screw micro-compounder, the viscosity curves for SEBS and SMP were obtained, from which power-law fit parameters (K, n) can easily be estimated. In this work, for demonstration purpose, only the SEBS data have been presented. Figure 2b shows the flow curves of SEBS at 220 °C temperature with the power-law fit parameters estimated as $K = 1560$ and $n = 0.8254$. Using these power-law fit parameters and the geometric parameters of the screw system into Eq. (5), the pressure flow equation of SEBS can be reduced to Eq. (6), assuming that the pressure gradient is linear over the screw length ($L_{\mathrm{A}} = 0.18$ m):

$$\left(Q_{\mathrm{p}}\right)_{\mathrm{Extruder(SEBS)}} = 3.33 \times 10^{-14} \times \sqrt[0.8254]{(\Delta P)_{\mathrm{Extruder}}}\ \mathrm{m}^3/\mathrm{s}. \tag{6}$$

Since the screw system does not have any wear and has a very small clearance ($\delta = 0.0005$ m) between the flight surfaces and the barrel surface, the leakage flow will be very small and be neglected in this study.

In addition to the flow components inside the screw-barrel system, there is another melt flow that arises from the pressure gradient developed inside the heated hose. This pressure gradient also reduces the overall melt flow and can be mathematically modeled using the fundamentals of pipe flow [28] applying to power-law polymer melt as derived in the supplementary information and given in the following equation for a hose with an internal radius of R:

$$\left(Q_{\mathrm{p}}\right)_{\mathrm{Heated\ Hose}} = \frac{n\pi}{(3n+1)} \times \sqrt[n]{\frac{1}{2K}\left(\frac{\mathrm{d}p}{\mathrm{d}L}\right)_{\mathrm{Heated\ Hose}}} \times (R)^{\left(\frac{3n+1}{n}\right)}. \tag{7}$$

Again, Eq. (7) can be re-written for SEBS flowing through the heated hose. However, the temperature of the flexible tube is 210 °C for SEBS which is different than that of the pellet extruder. Therefore, a new set of power-law fit parameters ($K = 2113$ and $n = 0.8384$) for 210 °C estimated from Fig. 2b must be used in Eq. (7) for 2-foot-long ($L_T = 0.61$ m) hose with internal radius, $R = 1.5875$ mm. That reduces the Eq. (7) as follows:

$$\left(Q_p\right)_{HeatedHose} = 1.17 \times 10^{-16} \times \sqrt[0.8384]{(\Delta P)_{HeatedHose}}\ \mathrm{m}^3/\mathrm{s}. \tag{8}$$

Finally, the total melt flow can be expressed by the following single equation:

$$Q_{\mathrm{Total}} = Q_{\mathrm{d}} - \left(Q_{\mathrm{p}}\right)_{\mathrm{Extruder}} - \left(Q_{\mathrm{p}}\right)_{\mathrm{Heated\ Hose}}, \tag{9}$$

which can again be written for SEBS as follows:

$$\begin{aligned} Q_{\mathrm{Total}} = {} & (3.3 \times 10^{-8} N) - 3.33 \times 10^{-14} \\ & \times \sqrt[0.8254]{(\Delta P)_{\mathrm{Extruder}}} - 1.17 \times 10^{-16} \\ & \times \sqrt[0.8384]{(\Delta P)_{\mathrm{Heated\ Hose}}}. \end{aligned} \tag{10}$$

This equation can be used to determine the screw speed in rpm for a desired flow rate or print speed. However, it requires an experimental measure of the pressure drop across both the extruder and the heated hose, for accurate estimation. However, due to a relatively small pressure drop at lower screw speeds, by considering only the drag flow, the first term of the Eq. (10), one may get an approximate relation between desired print speed and required screw speed using the following equation:

$$\text{Print speed}, S = \frac{Q_{\mathrm{d}}}{\pi\left(r_{\mathrm{nozzle}}\right)^2}. \tag{11}$$

2.4 Pellet extrusion

The process of pellet extrusion requires setting and maintaining temperatures of three major components of this system. This set of temperatures may vary for different materials, i.e., SEBS and SMP, in this work. Some initial tests were conducted to fine-tune the process and identify this

Table 1 Printing parameters for SEBS and SMP extrusion

	SEBS	SMP
Temperature of the pellet extruder (°C)	220	200
Temperature of flexible heated tube (°C)	210	190
Temperature of printing head (°C)	220	200
Nozzle sizes (mm)	0.35, 0.5, and 1.0	

set of temperatures for both materials to obtain continuous defect-free extrudates. Table 1 lists the sets of temperature for both SEBS and SMP which resulted in high-quality extrusion. The temperature of the heated hose was kept at a lower temperature than the pellet extruder and print head, that is 20 °C below the maximum temperature limit (230 °C) of the PTFE core of the heated hose. Figure 2c shows the actual print speed or extrusion rate of the FPP system at different screw speed using a 0.5 mm nozzle diameter. This plot clearly shows that the extrusion rate tends to reach a plateau at higher screw speed due to the pressure-driven backflows developed which were not experimentally measured in this work. The maximum screw speed attainable with the pellet extruder setup was approximately 6 rpm where the supplier's specification of maximum screw speed was 8 rpm. This analysis was performed to identify the suitable screw speed for desired print speed. Hence, for accurate measurements, two pressure transducers installed across the pellet extruder and flexible tube would be highly recommended for future work. Based on these trials, a print speed of 30 mm/s was chosen for printing when using a 0.5 mm nozzle and setting the screw speed to 3 rpm.

2.5 Dynamics of the heated hose

As the heated hose is the main element of this system for transporting the polymer melt from the pellet extruder to the print head, we also consider the flow of polymer melt inside this heated hose, because it may put an additional limit on the print speed and power requirements.

2.5.1 Melt properties

Polymer melts have highly non-linear, shear rate-dependent viscosity properties. The shear rate is determined by the flow rate and the geometry of the tube and the apparent shear rate $\left(\dot{\gamma}_{\text{app}}\right)$ for a power-law polymer melt can be estimated using the following equation [25]:

$$\dot{\gamma}_{\text{app}} = \frac{4Q_{\text{Total}}}{\pi(R)^3}\left(\frac{3n+1}{4n}\right). \tag{12}$$

For a print speed of 30 mm/s with SEBS and using a 0.5 mm nozzle, the apparent shear rate at the channel wall of the heated hose was calculated as 1.875 s^{-1}. This shear rate, at the temperature of 210 °C, corresponds to the viscosity of 1909 Pa s, estimated using the power-law fit equation from the viscosity curve given in Fig. 2b.

2.5.2 Heat flux requirements

Since the polymer is in its molten state before entering the heated hose, ideally, it would be an adiabatic process to transport the melt to the print head, if there is no heat loss. However, in practice, though 3-mm-thick fiberglass insulation was applied on the outer surface of the hose, there is still some heat loss to the environment. This heat loss is compensated for using an external band heater which supplies a variable heat flux to maintain the desired temperature of the heated hose.

2.5.3 Pressure drop estimation

From a momentum balance on the heated hose, the pressure drop across it can be predicted as performed for an extrusion die [6]. By solving both momentum and energy balances, the pressure drop within the liquefier of a 3D printer was modeled by Ramanath et al. [5], which can be used for determining the pressure drop across the heated hose. Hence, the equation has been re-written as follows:

$$\Delta P_{\text{Heated Hose}} = \frac{2L_{\text{T}}K}{R^{3n+1}} \times \left[\frac{(3n+1)Q_{\text{Total}}}{\pi n}\right]^n \times e^{\left[\alpha\left(\frac{1}{T}-\frac{1}{T_\alpha}\right)\right]}. \tag{13}$$

All the parameters are already discussed in the previous sections except T for the temperature of heated hose, α for activation energy, and T_α for a reference temperature where the temperature dependence of the melt viscosity disappears. This model was developed with some assumptions [29]: (a) the melt is incompressible, (b) the flow is laminar, fully developed and steady state, (c) shear rate dependence of the viscosity can be expressed using the power-law model, and (d) melt viscosity also depends on temperature and follows the Arrhenius model. We also do not consider any axial or radial expansion of the hose in this analysis.

2.6 Printing of SEBS soft robotic actuator

FPP system has the potential to revolutionize the field of soft actuators through its capacity to directly print very soft, stretchable thermoplastic materials. Figure 3a shows a soft, flexible octopus printed with SEBS that has stretchable arms extensible over 300% without failure. The 3D model of the octopus was downloaded from thingiverse.com and designed

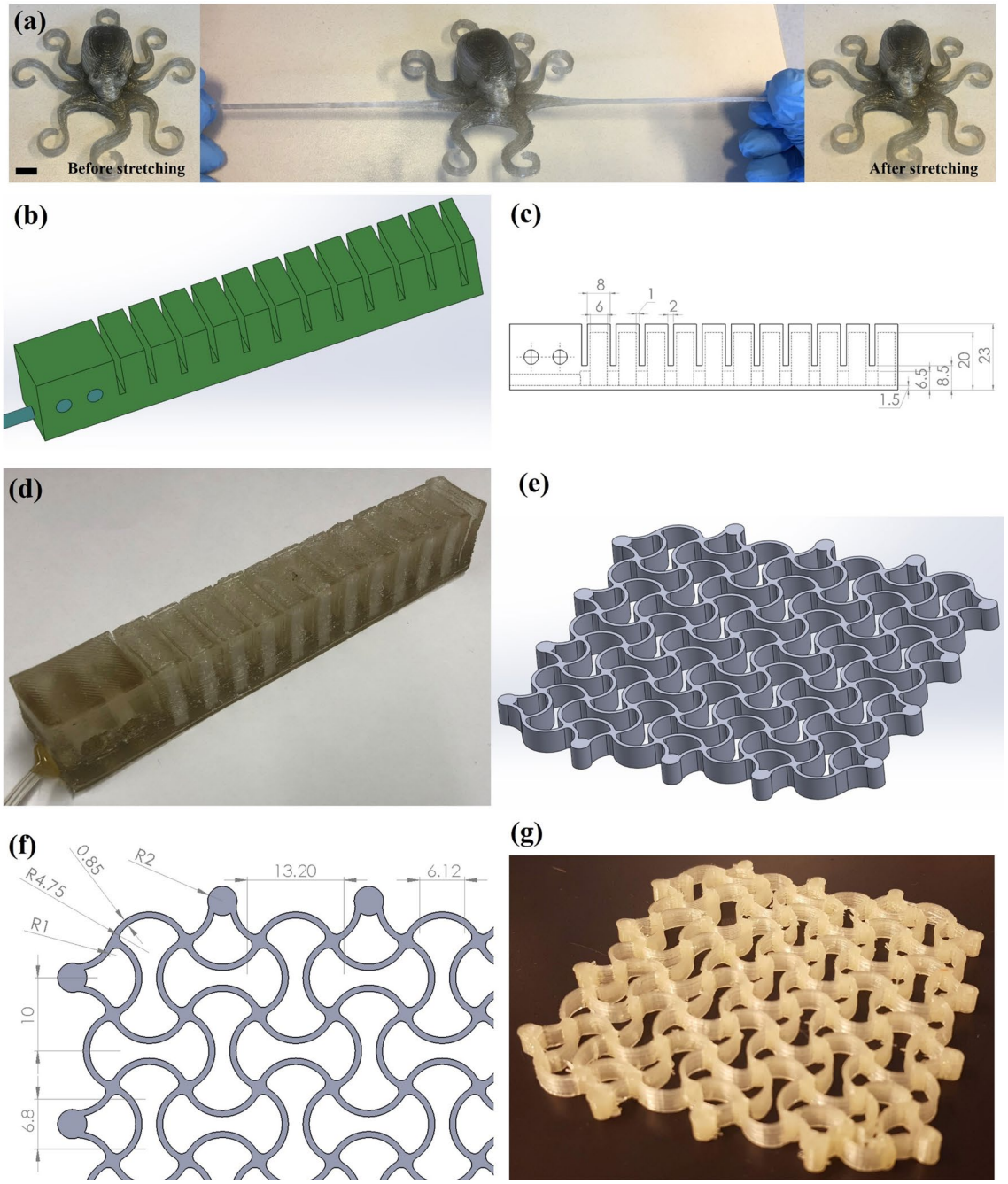

Fig. 3 **a** A stretchable octopus with 300% stretchable arms without any mechanical failure. The 3D model (**b**) of the soft actuator with dimensions presented in (**c**). The photograph of the actual actuator shown in (**d**). **e** The 3D model of the auxetic structure with dimensions presented in (**f**). The printed structure is depicted in (**g**). All dimensions in 3D models are in mm

by *Laurens kempjes*. Commercially available flexible filaments can be directly used to print objects with limited flexibility, but are not as reversibly stretchable as the SEBS used here. This ability to print very stretchable devices opens up new possibilities in 3D printing applications such as soft robots where extreme deformations over many cycles are needed.

Inspired by the ability of soft-bodied biological systems to interact with the uncertain environment and achieve compliant motion without multiple mechanical joints, many recent works focus on soft robotic actuators [30, 31]. Therefore, to demonstrate the performance of the FPP system, we choose to print soft robotic actuators made of SEBS. In this work, the pneumatic network

(PneuNet)-based soft robots were designed inspired by work done by the Whitesides Group at Harvard University [32]. This actuator has channels and reservoirs embedded into the elastomeric materials which can be inflated using pressurized air to achieve mechanical actuation. The 3D model of the soft robotic actuator is shown in Fig. 3b, and c, whereas its actual printed version is shown in Fig. 3d.

Inherently, FDM parts have poor surface quality due to the staircase effect and chordal error while slicing the object [33]. FDM parts are not usually airtight in their 3D volume, and air gaps between deposited fibers and layers contribute to fluid leakage throughout the printed body. This limits the feasibility of FDM technology in printing PneuNet-based soft robotic actuators. However, this issue may be overcome by selecting proper layer height, layer width, and printing temperature to enhance the fusion between deposited fibers and layers. An additional annealing process may also contribute in relieving the residual thermal stress if heated sufficiently higher than glass the transition temperature (T_g) to allow the material to re-flow, filling the voids between fibers or layers. As a result, an airtight 3D printed part may be realized with substantially reduced voids in its 3D volume. Hence, after printing the soft robotic actuators of SEBS, if required, they were also heat treated at 135 °C for 30 min.

2.7 Printing of SMP auxetic structure

In addition to the pellets of soft materials, the FPP system is also capable of printing pellets of rigid polymers if the pellets are less than 5 mm in size in any of the dimensions [22]. To demonstrate this capability, rigid pellets of SMP were used to print functional devices like re-entrant structures. Such structures are getting increasing attention for their ability to unlock "4D" printing capabilities and morphable metamaterials, but have mainly been prototyped via proprietary resins or more expensive additive manufacturing processes [34]. Re-entrant structures have auxetic behavior due to their negative Poisson's ratio, which is of great interest due to their counter-intuitive behavior under deformation [35]. Using SMP materials, their thermo-mechanical coupling is utilized in re-entrant auxetic structures for controllable one-way actuation [36]. The degree of auxeticity is determined by the particular geometry of the material system and its deformation mechanism when loaded. Higher auxetic performance often requires complex geometry [37]. Complex auxetic structures generally involve time-consuming and complicated fabrication techniques; hence, rapid prototyping technologies may be useful to fabricate such material systems [35]. A re-entrant auxetic structure with sinusoidal connectors inspired by the design used by Dolla et al. for drug diffusion [38] has been printed with SMP to demonstrate proof-of-principle for our system to be used for this purpose. Figure 3e shows the 3D model of the sinusoidal auxetic structure with dimensions of its unit cell in Fig. 3f, and the actually printed structure is shown in Fig. 3g.

3 Results and discussion

3.1 Thermal simulation of the heated hose

The insulated, heated hose was assumed to be a hot vertical tube having a uniform diameter of 20 mm. The tube was further considered to be in a free convection situation where the temperature of the heating element is kept fixed at 210 °C. The connectors on both ends of the hose were assumed to have a uniform fixed temperature of 220 °C. Since a 4-foot (1.22 m)-long heater band (15 mm wide) was wrapped on to the 2-foot-long hose, it is reasonable to assume the heater as a continuous annular tube fitted on the hose. With these assumptions, first, the constants of the Hilpert correlation (C, m) were estimated for laminar free convection over a slender circular cylinder as developed by Cebeci [39]. Finally, the convective film coefficient (h) of 22.0 W/m^2 °C was estimated using the following equation:

$$Nu = \frac{hL}{k} = C(Gr_L Pr)^m, \tag{14}$$

where Nu, Gr_L, and Pr are the Nusselt number, Grashof number, and Prandtl number, respectively, of the air flow around the heated hose. L and k are the characteristics length and thermal conductivity of the flexible tube. Then, the thermal analysis was performed in ANSYS, as shown in Fig. 4a, b. In this steady-state thermal simulation, the temperature of the surrounding environment was assumed to be 25 °C. Figure 4a shows temperature distribution along the radial direction (cross-sectional) of the heated hose. It indicates that the core Teflon tubing is nearly 220 °C and the temperature of its outer surface is just more than 120 °C which was experimentally measured as ~ 110 °C. From the thermal simulation, the temperature distribution along the axis of the heated hose was found to be approximately uniform except a slight temperature variation near the ends of the tube. Figure 4b illustrates the temperature distribution in the tri-extruder, which required the estimation of convective film coefficient (h) of the forced convection around the heat-sink of one input of the tri-extruder, as performed in previous work [24].

3.2 Ultimate strength of extrudates

When the materials were successfully extruded using the FPP system, the extrudates were characterized to analyze

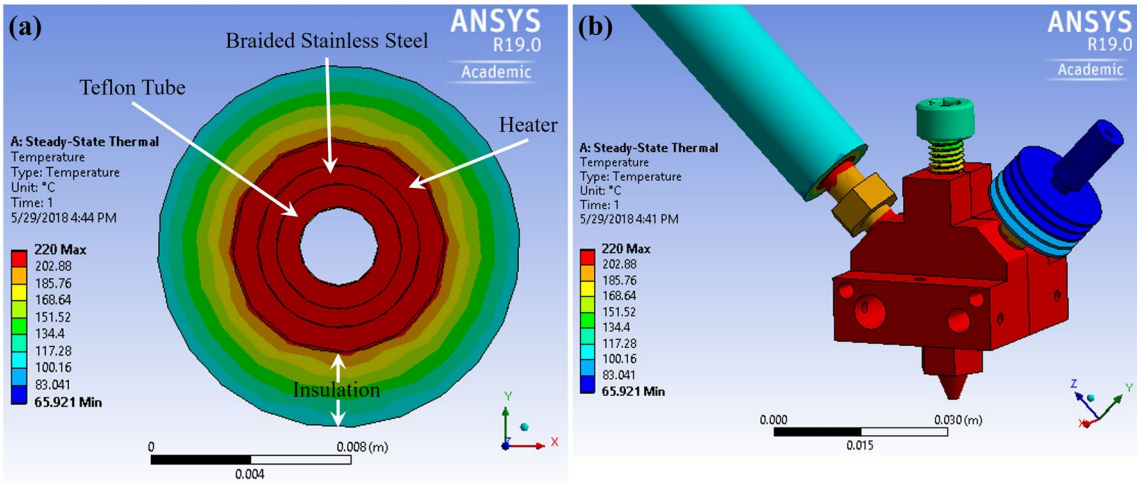

Fig. 4 The temperature distribution across the **a** cross-section of the heated hose and **b** at the end connector with the tri-extruder, from the thermal simulation using ANSYS

Table 2 Experimental results from tensile testing of the extrudates

Materials	Nozzle diameter (mm)	Extrudate diameter (mm)	Tensile strength (MPa)	Elongation at break (%)
SEBS	0.35	0.33 ± 0.01	12.5 ± 2.2	850 ± 70
	0.50	0.52 ± 0.02	11.1 ± 1.8	875 ± 78
SMP	0.35	0.36 ± 0.01	33.2 ± 2.3	32 ± 1.4
	0.50	0.54 ± 0.03	35.0 ± 3.6	34 ± 2.1

their mechanical properties. The printer was allowed to extrude the material from a height of approximately 10 cm above the print bed, so that when the free extrudate touches the bed, it is already solidified. These extrudates were then tested in a custom test setup reported elsewhere [24] to measure ultimate tensile strength (UTS) and elongation at break. Since elongation at break of the SEBS extrudates was significantly higher than the elongation range of the reported test setup, they were tested in a different approach. First, a specified length of the SEBS extrudate was hung from an analog mass balance and the other end of the extrudate was pulled down until the extrudate failed. The whole process was video recorded, which was later used to estimate the elongation at break and the length of extrudate when the failure occurred. Table 2 summarizes the extrudate diameter, UTS, and elongation at break for both SEBS and SMP extrudates. Each measurement was repeated five times. The SEBS extrudates could stretch to more than 800% which is higher than the reported stretchability (~ 600%) of bulk SEBS [20]. This phenomenon may be explained by the increased linearity of the polymeric chains from an extrusion process [25].

3.3 Effect of printing parameters on airtight SEBS structure

The major printing parameters affecting the size and number of inter- and intra-layer voids were found to be layer height and layer width. These settings are defined in the slicing step when the 3D model is converted to a number of 2D layers. In this work, an open source slicing program, Slic3r [40], was used for the slicing step. A number of small actuators with only three hollow chambers, as shown in Fig. 5b, were printed with different layer widths and heights. Then, pressurized air was applied to inflate them until they ruptured to measure the air pressure (gage) which causes pneumatic failure. The microscope images of chamber walls of the samples were also examined to study the voids present in those samples. Figure 5c shows the printing parameters needed to achieve airtight SEBS walls when using a 0.5 mm nozzle. There are three distinct regions in the plot; printing of SEBS structures in the first region deposits the material with a "squashed" cross-section rather than a more typical circular cross-section. It also causes a degree of over-extrusion to help to fill the possible voids between the deposited fibers. These phenomena contribute to airtight FDM parts with minimal voids in their 3D volume. Because the SEBS is a clear material, the boundary effect of the internal layers also disappears, leading to a more transparent printed part. Figure 5e shows a part with 20 mm depth, still transparent enough to read text through this thickness.

The second region in Fig. 5c represents the print settings that result in an object which is mostly airtight except for some random air-leaking locations. These printed parts require an additional heat treatment process to allow the

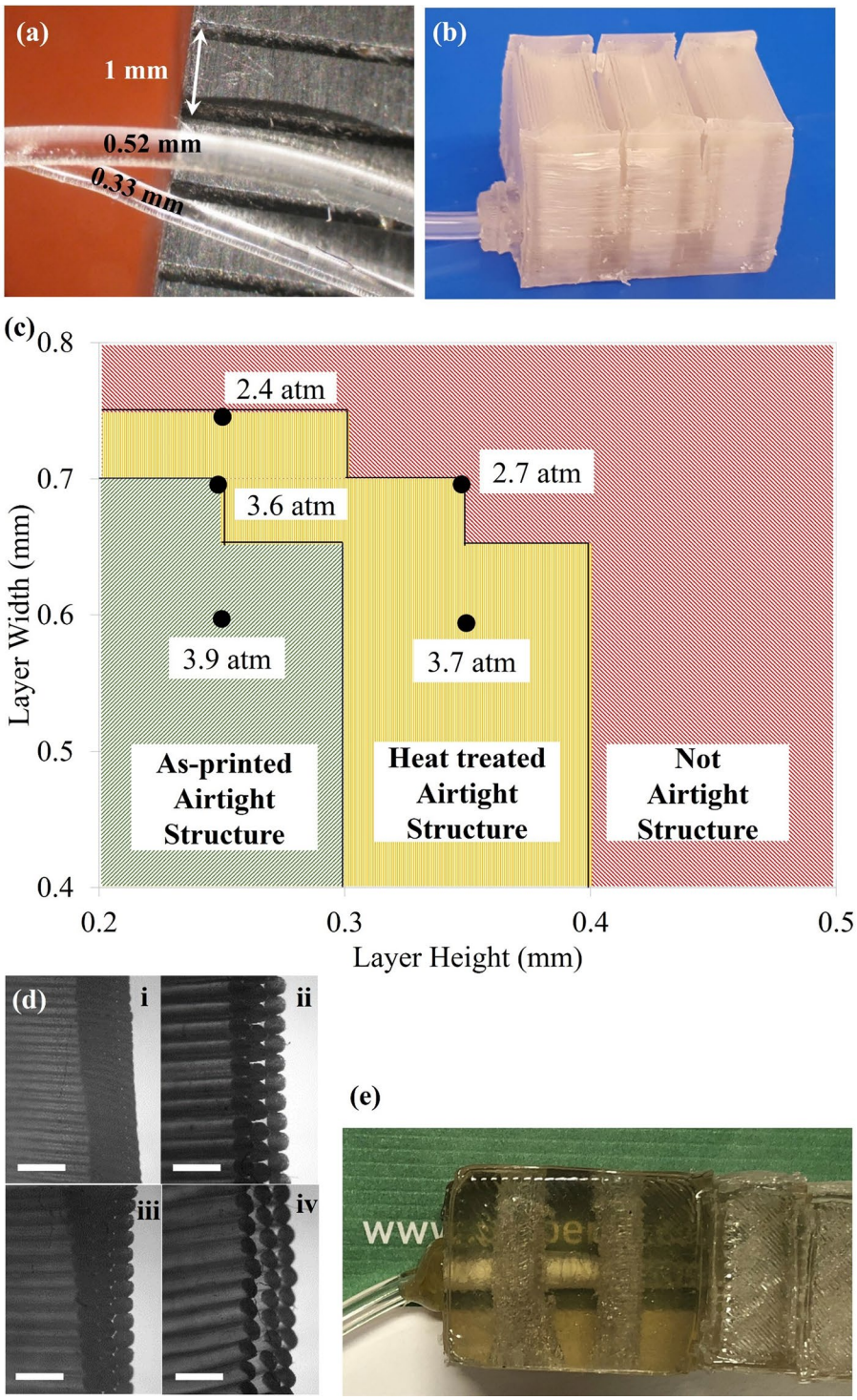

Fig. 5 **a** Microscope images of two representative SEBS extrudates from 0.5 and 0.35 mm nozzles; a metric scale is in the background. **b** A small actuator with only three chambers printed with SEBS was used to determine the effect of printing parameters on airtightness of soft robots; **c** a graphical representation of the effect of printing parameters on airtightness of printed walls. Three distinct regions printing parameters which result in as-printed airtight structure, heat-treated airtight structure, and not airtight structure. Data points represent the air pressure which causes rupturing leading to fluid leakage through the chamber walls. **d** Microscope images of the cross sections of samples printed with 0.6 mm layer width and (i) 0.25 mm layer height, (ii) 0.35 mm layer height (before heat treatment), (iii) 0.35 mm layer height (after heat treatment), and (iv) 0.45 mm layer height (Scale bars are 1.5 mm). **e** The base of the SEBS actuator printed with 0.25 mm layer height and 0.5 mm layer width, resembling the bulk SEBS material with high optical transparency

materials to re-flow—filling up the unwanted voids or sealing up the cracks. It was experimentally determined that if an SEBS part printed with parameters defined by the region B undergoes a heat treatment at 135 °C for 30 min, it becomes airtight, suitable for pneumatic applications. The third region has too many voids for the part to become airtight even with the heat treatment step.

Five small actuator samples printed with SEBS were tested to determine the maximum air pressure before rupturing. Once a sample was ruptured it went through an additional heat treatment process (135 °C for 30 min) to seal the crack and tests were repeated five times. Figure 5c also shows the average air pressure which caused the actuator chamber to rupture. It shows that the samples

printed with parameters corresponding to the first region (without heat treatment) and the second region (with heat treatment) have statistically indistinguishable rupturing pressure.

3.4 Performance of SEBS soft actuator

Once the SEBS soft robotic actuator has been directly printed, it was characterized to measure the actuator force and the tip deflection induced for a range of air pressure (gage) applied to its PneuNet. The custom setups in Fig. 6a,

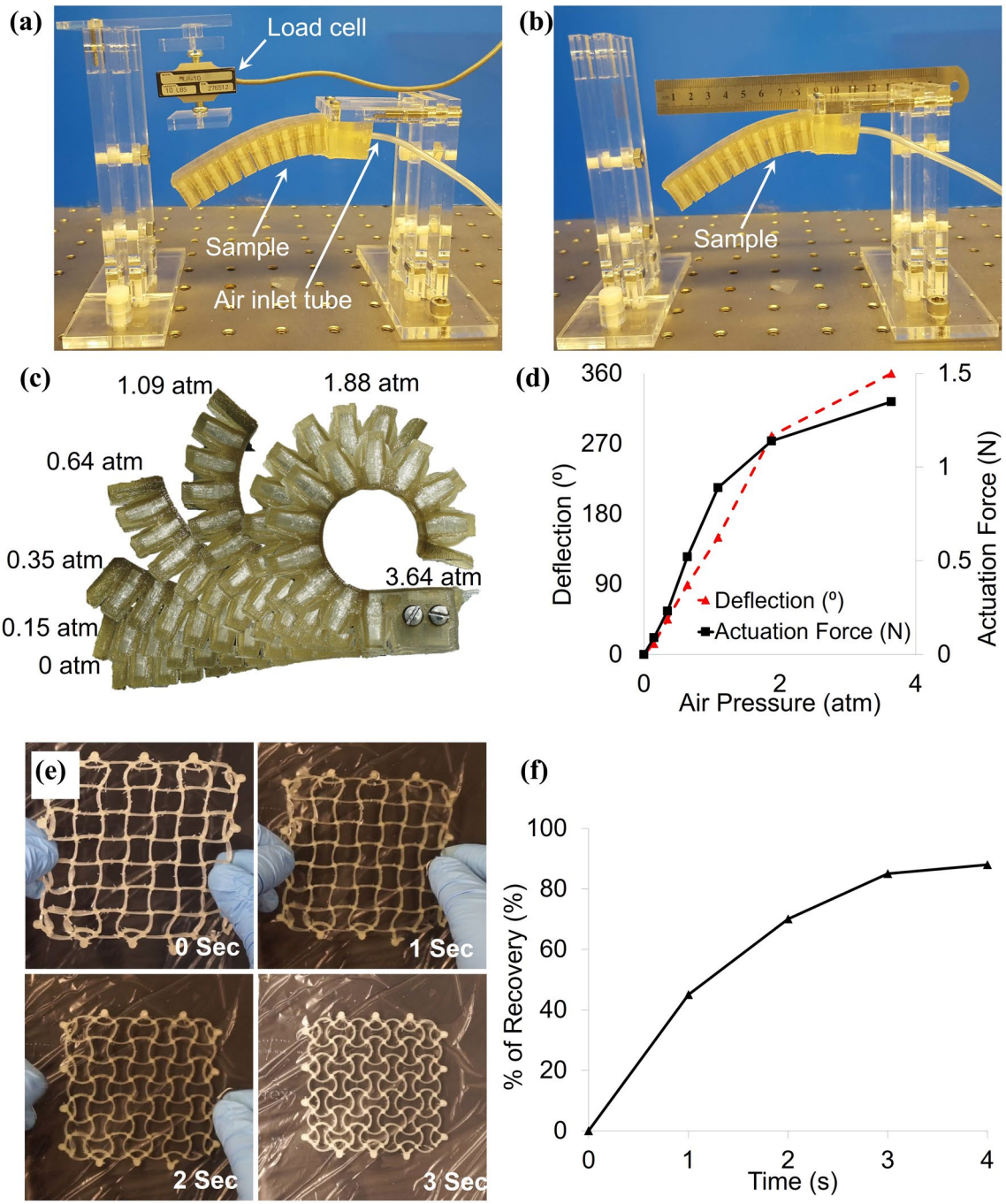

Fig. 6 The custom setups for measuring the **a** actuation force and **b** tip deflection of the SEBS soft robotic actuator. **c** Different states of actuation of a representative SEBS soft robot. **d** The dependences of the actuation force and deflection angle plotted against the air pressure applied. **e** Time-lapsed photos of sinusoidal re-entrant structure showing its shape recovery and **f** the % recovery of the as-printed re-entrant structure over the period of recovery

b with acrylic holders were used to characterize the actuator. A National Instrument data acquisition (DAQ) hub (NI USB-6289) along with a Windows Presentation Foundation (WPF) application written in C# and a load cell (Transducer Techniques, MLP-10) was used to measure the actuation force. To measure the tip deflection of the actuator, a camera was used to take photos of the deflected actuator. These photos along with image processing software were used to measure the angle of deflection of the actuator tip. Figure 6c shows the different states of actuation of the soft robotic actuator displaying corresponding air pressure (gage). A graph showing the dependence of actuation force and tip deflection of the actuator on the air pressure applied is presented in Fig. 6d.

3.5 Recovery of SMP auxetic structure

Previous 3D printing of SMP was recently reported where researchers first used a pellet extruder to fabricate SMP filament, which was then used in FDM systems to print SMP devices following with an annealing process before utilizing the shape memory property [41]. However, in this work, the SMP auxetic structures were printed directly from its pellets using the FPP system and did not require a post-processing heat treatment step. Figure 6e shows time-lapsed photos of the sinusoidal re-entrant auxetic structure (size: 8 cm × 8 cm × 5 mm) depicting its shape memory property. First, the as-printed structure ($T_g = 35$ °C) was heated to 40 °C under hot water and stretched 2 cm along both length and width direction (deformed size: 10 cm × 10 cm × 5 mm). Then, it was cooled down to room temperature and kept for 2 min while maintaining the deformed shape. To observe the recovery, the object was then put again under hot water of ~ 50 °C, ($T_g + 15$ °C) recommended by Raasch et al. [41]. The % recovery was calculated based on the overall length of the auxetic structure, as shown in Fig. 6e and using the following equation:

$$\%\text{Recovery} = \frac{\left(L_{\text{deformed}} - L_{\text{current length}}\right)}{\left(L_{\text{deformed}} - L_{\text{original}}\right)} \times 100\%, \qquad (15)$$

where L_{deformed} = the length of the deformed and cooled down structure, L_{original} = the original as-printed length of the structure and $L_{\text{current length}}$ = the current length of the structure. Figure 6f shows the % Recovery of the auxetic structure over a period of time, where it is clearly shown that the structure returns to around 8.1 cm on both length and width directions which is equivalent to 95% recovery. In addition to the auxetic structure, a number of prototypes were also printed using this system. The movie file in the supplementary information shows recovery of a "UofA" object under 50 °C hot water.

4 Conclusions

To the authors' best knowledge, this is the first time that material extrusion-based 3D printing has been demonstrated directly from pellets using a flexible heated hose as the feed mechanism. Since the pellet extruder is fixed, while the print head moves, it decouples the power/heating limitations from the speed/resolution needs of the printer hot end. Using this FPP technology, industrial-scale extruders coupled to FDM printers could deposit materials, in future, with properties and deposition rates previously impractical. While the motivating drive for the development of this technology was to solve the issue of working with extremely soft elastomers partially, the effective feed speeds achievable and economic savings of direct pellet extrusion can make the heated hose-based extrusion a very valuable improvement to all FDM-type printers.

Acknowledgements This work was funded by Natural Sciences and Engineering Research Council of Canada (NSERC).

Compliance with ethical standards

Conflict of interest On behalf of all authors, the corresponding author states that a startup company has been founded to help commercialize portions of the technology disclosed within this article.

References

1. Srivatsan TS, Sudarshan TS (2015) Additive manufacturing: innovations, advances, and applications. CRC Press, Boca Raton
2. Turner BN, Scott AG (2015) A review of melt extrusion additive manufacturing processes: II. Materials, dimensional accuracy, and surface roughness. Rapid Prototyp J 21:250–261
3. Elkins K, Nordby H, Janak C, Gray RW, Bohn JH, Baird DG (1997) Soft elastomers for fused deposition modeling., The University of Texas in Austin, Laboratory for Freeform Fabrication and University of Texas at Austin, pp 441
4. Bellini A, Guceri S, Bertoldi M (2004) Liquefier dynamics in fused deposition. J Manuf Sci E-T ASME 126:237–246
5. Ramanath HS, Chua CK, Leong KF, Shah KD (2008) Melt flow behaviour of poly-epsilon-caprolactone in fused deposition modelling. J Mater Sci Mater Med 19:2541–2550
6. Michaeli W (2003) Extrusion dies for plastics and rubber. Carl Hanser Verlag GmbH & Co. KG, Göttingen
7. Yardimci MA, Guceri SI, Danforth SC (1997) Thermal analysis of fused deposition. August 11–13, Austin, TX, The University of Texas at Austin
8. Venkataraman N, Rangarajan S, Matthewson MJ, Harper B, Safari A, Danforth SC, Wu G, Langrana N, Guceri S, Yardimci A (2000) Feedstock material property—process relationships in fused deposition of ceramics (FDC). Rapid Prototyp J 6:244–253
9. NINJAFLEX®: the market leading flexible filament. https://ninjatek.com/products/filaments/ninjaflex/. Accessed 29 Nov 2017
10. PolyFlex. http://www.polymaker.com/shop/polyflex/. Accessed 29 Nov 2017
11. FlexSolid. http://www.madesolid.com/. Accessed 29 Nov 2017

12. Saari M, Galla M, Cox B, Krueger P, Cohen A, Richer E (2015) Additive manufacturing of soft and composite parts from thermoplastic elastomers. August 10–12, Austin, TX, The University of Texas at Austin, 949–958
13. TITAN Robotics. THE ATLAS. http://www.titan3drobotics.com/atlas/. Accessed 9 Oct 2018
14. Linthicum T, Simpson DS, Linthicum B et al, inventors, inventor; Sculptify LLC, assignee., assignee (2014) Extrusion system for additive manufacturing and 3-d printing. US patent US20150321419A1. Pending
15. Whyman S, Arif KM, Potgieter J (2018) Design and development of an extrusion system for 3D printing biopolymer pellets. Int J Adv Manuf Technol 96:3417–3428
16. Woern AL, Byard DJ, Oakley RB, Fiedler MJ, Snabes SL, Pearce JM (2018) Fused particle fabrication 3-D printing: recycled materials' optimization and mechanical properties. Materials 11:1413
17. Moreno Nieto D, Casal López V, Molina SI (2018) Large-format polymeric pellet-based additive manufacturing for the naval industry. Addit Manuf 23:79–85
18. Ajinjeru C, Kishore V, Liu P, Lindahl J, Hassen AA, Kunc V, Post B, Love L, Duty C (2018) Determination of melt processing conditions for high performance amorphous thermoplastics for large format additive manufacturing. Addit Manuf 21:125–132
19. Singamneni S, Smith D, LeGuen M, Truong D (2018) Extrusion 3D printing of polybutyrate-adipate-terephthalate-polymer composites in the pellet form. Polymers 10:922
20. Bschaden BS (2014) Developing design guidelines for improved gecko inspired dry adhesive. Dissertation, University of Alberta
21. Sameoto D (2017) Manufacturing approaches and applications for bioinspired dry adhesives. In: Heepe L, Xue L, Gord S (eds) Bio-inspired structured adhesives. Springer, Cham, pp 221–244
22. FILUSTRUDER. Available from: https://www.filastruder.com/products/filastruder-kit. Accessed 20 Mar 2018
23. Khondoker MAH, Sameoto D (2016) Design and characterization of a bi-material co-extruder for fused deposition modeling. November 11–17, Phoenix, AZ, USA, The American Society of Mechanical Engineers, IMECE2016-65330-9
24. Khondoker MAH, Sameoto D (2017) Printing with mechanically interlocked extrudates using a custom bi-extruder for fused deposition modelling. Rapid Prototyp J 24:921–934
25. Morton-Jones DH (1989) Polymer processing. Chapman and Hall, New York
26. Crawford RJ (1981) Plastics engineering. Butterworth-Heinemann, Oxford
27. Stevens MJ, Covas JA (1995) Extruder principles and operation. Springer Science + Business Media, Berlin
28. Munson BR, Okiishi TH, Huebsch WW, Rothmayer AP (2013) Fundamentals of fluid mechanics. Wiley, New York
29. Turner BN, Strong R, Gold SA (2014) A review of melt extrusion additive manufacturing processes: I. Process design and modeling. Rapid Prototyp J 20:192–204
30. Hannan MW, Walker ID (2003) Kinematics and the implementation of an elephant's trunk manipulator and other continuum style robots. J Rob Syst 20:45–63
31. Laschi C, Cianchetti M, Mazzolai B, Margheri L, Follador M, Dario P (2012) Soft robot arm inspired by the octopus. Adv Rob 26:709–727
32. Bobak M, Panagiotis P, Christoph K, Sophia W, Shepherd RF, Unmukt G, Jongmin S, Katia B, Walsh CJ, Whitesides GM (2014) Pneumatic networks for soft robotics that actuate rapidly. Adv Funct Mater 24:2163–2170
33. Pandey PM, Venkata Reddy N, Dhande SG (2003) Improvement of surface finish by staircase machining in fused deposition modeling. J Mater Process Technol 132:323–331
34. Wagner M, Chen T, Shea K (2017) Large shape transforming 4D auxetic structures. 3D Print Addit Manuf 4:133–142
35. Liu Y, Hu H (2010) A review on auxetic structures and polymeric materials. Sci Res Essays 5:1052–1063
36. Rossiter J, Takashima K, Scarpa F, Walters P, Mukai T (2014) Shape memory polymer hexachiral auxetic structures with tunable stiffness. Smart Mater Struct 23:045007
37. Grima JN, Alderson A, Evans KE (2005) Auxetic behaviour from rotating rigid units. Phys Stat Solidi (b) 242:561–575
38. Dolla WJ, Fricke BA, Becker BR (2006) Structural and drug diffusion models of conventional and auxetic drug-eluting stents. J Med Devices 1:47–55
39. Cebeci T (1974) Laminar-free-convective-heat transfer from the outer surface of a vertical slender circular cylinder. September 3–7, Tokyo, Japan, Society of Heat Transfer of Japan, 15–19
40. Slic3r—G-code generator for 3D printers. http://slic3r.org/download. Accessed 17 Nov 2017
41. Raasch J, Ivey M, Aldrich D, Nobes DS, Ayranci C (2015) Characterization of polyurethane shape memory polymer processed by material extrusion additive manufacturing. Addit Manuf 8:132–141